Accuracy of large-scale cable-driven parallel robot with universal joint pulleys

Thibaut Paty, Nicolas Binaud, Florian Bugarin, Stéphane Segonds

Noname manuscript No.
(will be inserted by the editor)

Accuracy of large-scale cable-driven parallel robot with universal joint pulleys

Thibaut PATY · Nicolas BINAUD · Florian BUGARIN · Stéphane SEGONDS

Received: date / Accepted: date

Abstract Additive Manufacturing (AM) for building construction is booming because it is a cost-saving method. However, the means currently used do not offer a lot of flexibility. In order to adapt to different building geometries, the mechanical architecture that drives the printhead must be able to adapt easily to its environment. Cable-Driven Parallel Robots (CDPRs) might be an alternative to offer this adaptability to large-scale AM. In this context, the general aim is to develop a CDPR architecture for large-scale AM applications. CDPRs are not accurate because the use of cables makes the architecture less rigid. Taking into account the cable deformation can reduce this inaccuracy. However, the variation in Young's moduli of the cables due to hysteresis loop is very difficult to quantify in real time. In addition, the use of CDPRs for large-scale applications can generate large forces in the pulleys. The CDPR studied in this paper is designed with universal joint pulleys that minimize internal stresses. This paper deals with the accuracy of large-scale CDPR taking into account universal joint pulleys, the total deformation of the cables and the uncertainty on their Young's moduli. The aim is to theoretically validate the use of CDPRs for housing AM. First, the full geometrico-catenary model of CDPR is presented. Secondly, the detailed mechanical design of the universal joint pulley is performed. Then, a stress analysis validates the use of the universal joint pulley. Finally, an analysis of the accuracy of the printhead shows that in some areas of the accessible static workspace, a CDPR can be used for large-scale AM.

Keywords Cable-driven parallel robot · Pulley · Cable deformation · Large-scale additive manufacturing · Accuracy

T. PATY
3, rue Caroline Aigle F-31400 Toulouse CEDEX 04, France
Tel.: +33 (0)5 61 17 10 67
Fax: +33 (0)5 61 17 10 80
E-mail: thibaut.paty@univ-tlse3.fr

1 Introduction

In recent years, a lot of enhancements have been made to Additive Manufacturing (AM) methods [1]. As a result, it has been quickly adopted by the industry. In this context, the overall objective of this work is to develop a Cable-Driven Parallel Robots (CDPR) architecture for large-scale AM applications. The AM producing parts by depositing materials layer by layer, it creates the possibility to produce complex shapes without tools [2]. AM is applied in many fields such as aerospace, health care and construction. However, AM is currently limited by the size of the parts that can be produced. As a result, large-scale AM is a relatively recent field of research. One of the main applications of large-scale AM is building construction [3,4]. The most important challenges in AM for construction are to be able to create a robot with a large regular workspace, reconfigurable, easy to use, easily transportable and accurate enough to be able to move the printhead without collisions with its environment.

CDPRs can be a more effective solution for large-scale AM than classical rigid mechanisms [5]. During the last twenty years, many studies have been conducted on CDPRs for various applications [6]. CDPRs have a large workspace, a better load/weight ratio and a low cost with their architecture made up of cables, pulleys and a set of winches mounted to the ground [7]. In addition, they are sufficiently modular to be adapted to different environments. The feasibility of using CDPRs for the AM is well established [8,9]. However, they need to be further improved to be used in large-scale construction projects [10–12]. The architecture of a CDPR is made up of a rigid outer frame to which the actuators and idler pulleys are attached on. The CDPR also includes a Mobile Platform (MP) which is connected to the actuators by flexible cables only working in traction. In AM, the MP must carry the printhead. Suspended CDPRs have cables coming from above the MP and their number can be equal (non-redundant) or higher (redundant) than the number of Degrees of Freedom (DoF) of their associated MP [13–15]. In the case of suspended CDPRs, gravity plays an important role by pulling the MP downward and as a consequence keeping the cables in tension. A suspended CDPR architecture simplifies the problem of cable interference and does not use space on the ground as an added bonus. Using cables has advantages but it also comes with disadvantages. The main problems with CDPRs are the definition of their workspace [16,17] and their low accuracy [18,19]. In AM, low accuracy results in poor part quality. The low accuracy of CDPR is due to an accumulation of unavoidable geometrical and mechanical errors and uncertainties, such as: actuator accuracy, friction, stiffness, manufacturing tolerance intervals, functional clearances or non-linear cable behaviour. The effect of these uncertainties on the accuracy of CDPRs is not yet sufficiently quantified.

The present study focuses first on the design of a 3-DoF translational motions suspended CDPR [13,20], for large-scale applications and with universal joint pulley architecture [21]. From a mechanical point of view, this pulley is

almost not subject to flexion in its lever arm. Moreover, CDPR modelling is often performed using simplified models [22–24]. In order to quantify the positioning error of the MP a new detailed modelling of a suspended CDPR has been developed. This modelling takes into account the geometry and mass of the universal joint pulleys, the dead cable length between pulley and winch, as well as the elasticity and deflection of the cables. Indeed, the large-scale AM uses long cable lengths. The cable deflection must be considered [25]. Furthermore, due to the uncertainty on the cables' mechanical behaviour [26] (hysteresis phenomenon, cable aging, non-linear behaviour), the Young's modulus is considered to be non-constant and different between cables with the same initial parameters. Quantifying the MP positioning error is important to check the feasibility of large-scale AM with CDPR. This article presents three major contributions. First, the authors carries out a detailed geometric and mechanical modelling of a suspended CDPR. Secondly, he introduces a detailed universal joint pulley mechanical design for large-scale suspended CDPR and a stress analysis is carried out. Thirdly, the methodology can determine the maximum positioning error of the MP considering cables sagging and uncertainties on the cables' Young's modulus.

The paper is organized as follows: Section 2 deals with the CDPR modelling, Section 3 details the design of the suspended CDPR as well as the design and stress analysis of the universal joint pulleys. Finally, Section 4 shows the static workspace and quantifies the position error of the MP for large-scale AM applications.

2 CDPR modelling and MP position error

The first step is to define the models that will be used throughout the study. In this paper, CDPRs modelling takes into account the architecture and mass of the universal joint pulley as well as the elasticity, the mass and the overall length of the cables. For smaller CDPRs, the models often neglect the cable's mass and dead length. In addition, several existing models do not take into consideration the uncertainties on the cables' Young modulus. These uncertainties make it challenging to accurately position the MP in the workspace. In order to quantify this MP position error, the first step is to determine the initial cable's length with the inverse geometric model. Then use this length in the direct geometrico-catenary model with cable deflexion. Finally, the Young's modulus of the cables must be varied independently. It is then possible to determine the maximum MP position error when the mass and elasticity of the cables are neglected.

2.1 Inverse geometric model with universal joint pulley

For each MP position the inverse geometric model gives us the cable's total length. In this geometric model, the cables are not deformed.

2.1.1 CDPR parametrization with universal joint pulley

Figure 1 shows the setting of the universal joint pulley. This pulley can move on two rotations axes, whose parameters are α_i and β_i.

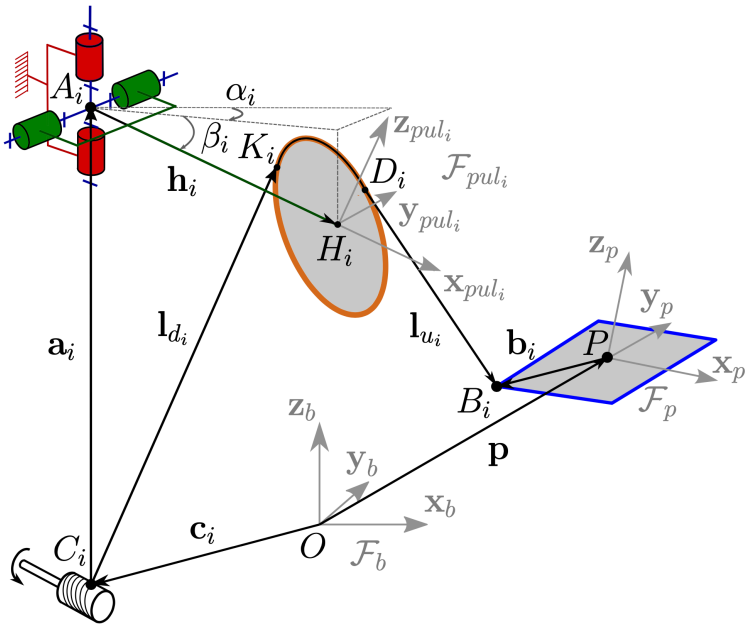

Fig. 1: Kinematics of universal joint pulley and CDPR parametrization

The frames of this parametrization are the base frame $\mathcal{F}_b$, the MP frame $\mathcal{F}_p$ and the pulley frame $\mathcal{F}_{pul_i}$, with $i = 1, \ldots, m$, and m the number of cables of the CDPR. The point O is the center of $\mathcal{F}_b$, the point P is the center of $\mathcal{F}_p$ and is the geometric center of the MP. The point H_i is the center of $\mathcal{F}_{pul_i}$ and is the geometric center of i^{th} pulley. C_i is the exit point of the winch. The point C_i is considered as a fixed point. The use of winches with an exit point of the cables imposed by a guide allows this assumption to be respected [27]. The point A_i is the center of rotation of the universal joint i^{th}. K_i and D_i are respectively the entry and exit point of the cable in the pulley. The position of these two points depends on the position of the MP in the workspace. B_i is the anchor point of the i^{th} cable on the MP. $\mathbf{a}_i$ and $\mathbf{c}_i$ are respectively the vectors pointing from C_i to A_i and from O to C_i. In the context of this study, the vector $\mathbf{a}_i$ is collinear with the axis $\mathbf{z}_b$. $\mathbf{p}$ is the position vector connecting the point O to the point P. The geometry of the MP is defined by the vectors $\mathbf{b}_i$ which connect the points P and B_i. $\mathbf{h}_i$ is the vector pointing from A_i to H_i. The length calculated by the 2-norm of the vector $\mathbf{h}_i$ is called the lever arm of the pulley. Finally, the dead cable's length l_{d_i} is 2-norm of the vector $\mathbf{l}_{d_i}$

pointing from point C_i to point K_i and the useful cable's length l_{u_i} is 2-norm of vector $\mathbf{l}_{u_i}$ pointing from point D_i to point B_i. Finally, in this parameterization the vectors $\mathbf{p}$, $\mathbf{c}_i$, $\mathbf{a}_i$, $\mathbf{l}_{d_i}$ and $\mathbf{l}_{u_i}$ are expressed in the base frame $\mathcal{F}_b$ and the vectors $\mathbf{h}_i$, $\mathbf{d}_i$ and $\mathbf{k}_i$ are expressed in the pulley's frame $\mathcal{F}_{pul_i}$.

2.1.2 CDPR static equilibrium with pulley mass

The calculation of the orientation angles of the universal joint, α_i and β_i, is necessary to determine the inverse geometric model. α_i is the orientation angle around $\mathbf{z}_b$ axis. β_i is the angle between the horizontal plane $(O, \mathbf{x}_b, \mathbf{y}_b)$ and $\mathbf{h}_i$. These two angles must respect the CDPR static equilibrium. With an universal joint, the pulley mass necessarily plays a role in the static equilibrium and therefore on the MP's final position. In order to focus the study on the MP's position and without allowing a loss of generality, CDPR with point-mass MP is studied in this paper. The points B_i are combined with point P [13,20,21]. Figure 2 shows the pulley positioning which respects the CDPR static equilibrium.

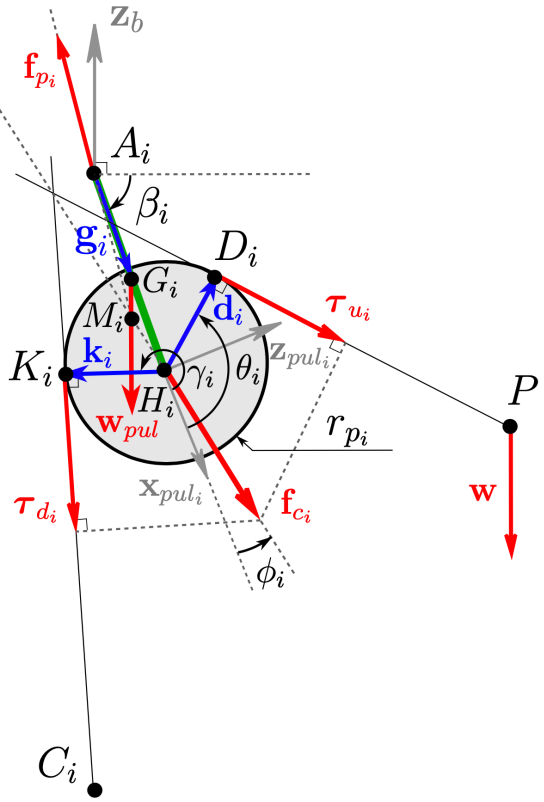

Fig. 2: Pulley static equilibrium in plane $(H_i, \mathbf{x}_{pul_i}, \mathbf{z}_{pul_i})$

It should be noted that the friction is neglected in this study. The MP weight is noted $\mathbf{w}$. The pulley mass is the sum of the sheave mass and the lever arm mass. r_{p_i} is the radius of the sheave. The vector $\mathbf{w}_{pul}$ representing the weight of the sheave+lever arm is applied to the gravity center G_i of the pulley. The vectors $\boldsymbol{\tau}_{u_i}$ and $\boldsymbol{\tau}_{d_i}$ represent the tension in the cables at both ends of the pulley's sheave and the vector $\mathbf{f}_{c_i}$ is the sum of the tension vectors. $\mathbf{f}_{p_i}$ is the holding force in the lever arm of the pulley. The pulley is a solid, subjected to three forces $\mathbf{w}_{pul}$, $\mathbf{f}_{c_i}$ and $\mathbf{f}_{p_i}$. The point M_i is the intersection of these three forces. In addition the entry point K_i and the exit point D_i of the pulley are defined by the vectors $\mathbf{k}_i$ and $\mathbf{d}_i$ and are a function of the angles γ_i and θ_i, respectively. The system unknowns are:

$$[\boldsymbol{\tau}_{u_i}, \boldsymbol{\tau}_{d_i}, \mathbf{f}_{c_i}, \mathbf{f}_{p_i}, \mathbf{h}_i, \mathbf{d}_i, \mathbf{k}_i] \quad \text{for } i = 1, \ldots, m \tag{1}$$

Geometrical and static equations are necessary to solve the inverse geometric model. First, the cable at the entrance and exit of the pulley must respect a tangency constraint. The scalar product between the tension vector $\boldsymbol{\tau}_{u_i}$ and the vector $\mathbf{d}_i$ must be null as well as the scalar product between the tension vector of the dead cable $\boldsymbol{\tau}_{d_i}$ and vector $\mathbf{k}_i$ Eq.(2).

$$\begin{cases} \boldsymbol{\tau}_{u_i}^T.\mathbf{d}_i = 0 \\ \\ \boldsymbol{\tau}_{d_i}^T.\mathbf{k}_i = 0 \end{cases} \quad \text{for } i = 1, \ldots, m \tag{2}$$

In addition, the pulley is considered to be mounted on bearings, allowing its rotation with minimal frictional torque around its axis of rotation. In this case, τ_{u_i} the 2-norm of vector $\boldsymbol{\tau}_{u_i}$ can be considered equal to τ_{d_i} the 2-norm of vector $\boldsymbol{\tau}_{d_i}$. The dead cable tension vector $\boldsymbol{\tau}_{d_i}$ can be expressed as follows:

$$\boldsymbol{\tau}_{d_i} = \tau_{u_i} \mathbf{u}_{d_i} \quad \text{for } i = 1, \ldots, m \tag{3}$$

Where $\mathbf{u}_{d_i}$ is the unit vector of the dead cable i. Moreover, the combined force $\mathbf{f}_{c_i}$ of the tensions $\boldsymbol{\tau}_{u_i}$ and $\boldsymbol{\tau}_{d_i}$ applying on point H_i can be expressed as:

$$\mathbf{f}_{c_i} = \boldsymbol{\tau}_{u_i} + \boldsymbol{\tau}_{d_i} \quad \text{for } i = 1, \ldots, m \tag{4}$$

According to the resultant static theorem applied to the pulley system, it is possible to write:

$$\mathbf{w}_{pul} + \mathbf{f}_{c_i} + \mathbf{f}_{p_i} = \mathbf{0} \quad \text{for } i = 1, \ldots, m \tag{5}$$

The static moment theorem of Newton's first law is apply on point A_i, which allows us to write that:

$$\mathbf{h}_i \times \mathbf{f}_{c_i} + \mathbf{g}_i \times \mathbf{w}_{pul} = \mathbf{0} \quad \text{for } i = 1, \ldots, m \tag{6}$$

Where $\times$ symbolizes the cross product operator and $\mathbf{g}_i$ is the vector between A_i and G_i. $\mathbf{g}_i$ is dependent of angles α_i and β_i. Finally, for the determination of cable tension vector $\boldsymbol{\tau}_{u_i}$, Newton's first law is expressed at point P as:

$$\mathbf{W}\boldsymbol{\tau} = -\mathbf{w} \tag{7}$$

Where $\boldsymbol{\tau}$ is the set of cables' tensions as $\boldsymbol{\tau} = [\tau_{u_1}, \ldots, \tau_{u_m}]^T$. $\mathbf{W}$ is the wrench matrix function of the MP's position. When there are more cables than DoF in the MP, the $\mathbf{W}$ matrix is not square. There are then several solutions to the $\boldsymbol{\tau}$ vector. The use of a tension distribution algorithm is essential. There are many algorithms developed to manage tensions [28,29]. In this paper and as in [30], the tension distribution algorithm minimizes the Euclidean norm of the sum of the tensions. Equation (8) shows the optimization problem.

$$\min \sqrt{\sum_{i=1}^{m} \tau_{u_i}^2} \tag{8}$$

However, some solutions are not acceptable because they display negative tensions or tensions that exceed the limit tension. The τ_{u_i} tensions of the useful cables must be limited as follows:

$$\begin{cases} \tau_{u_i} \geq \tau_{min} \\ \tau_{u_i} \leq \tau_{max} \end{cases} \tag{9}$$

Where $\tau_{min} > 0$. The optimization problem under constraints Eq.(10) is obtained in order to solve the CDPR static equilibrium.

$$\begin{cases} \min \sqrt{\sum_{i=1}^{m} \tau_{u_i}^2} \\ constraints: \\ \tau_{u_i} \geq \tau_{min} \\ \tau_{u_i} \leq \tau_{max} \\ \boldsymbol{\tau}_{u_i}^T.\mathbf{d}_i = 0 \\ \boldsymbol{\tau}_{d_i}^T.\mathbf{k}_i = 0 \\ \tau_{u_i}\mathbf{u}_{d_i} - \boldsymbol{\tau}_{d_i} = \mathbf{0} \\ \boldsymbol{\tau}_{u_i} + \boldsymbol{\tau}_{d_i} - \mathbf{f}_{c_i} = \mathbf{0} \\ \mathbf{w}_{pul} + \mathbf{f}_{c_i} + \mathbf{f}_{p_i} = \mathbf{0} \\ \mathbf{h}_i \times \mathbf{f}_{c_i} + \mathbf{g}_i \times \mathbf{w}_{pul} = \mathbf{0} \\ \mathbf{W}\boldsymbol{\tau} + \mathbf{w} = \mathbf{0} \end{cases} \tag{10}$$

Solving the optimization problem Eq.(10) is done by using the Matlab function "*fmincon*". After this optimization problem is solved, the positions of the pulley centres H_i are known. It is then possible to solve the inverse geometric model. To do this, the total cable's length L_{T_i} must be determined

for a MP position. L_{T_i} is the sum of the useful cable's length l_{u_i}, the dead cable length's l_{d_i} and the length of the cable wounded on the pulley (cf. Eq.(11)).

$$L_{T_i} = l_{u_i} + l_{d_i} + r_{p_i}(\gamma_i - \theta_i) \quad \text{for } i = 1, \dots, m \tag{11}$$

With $r_{p_i}(\gamma_i - \theta_i)$ the length of the cable wounded on the pulley i. l_{u_i} is 2-norm of vector $\mathbf{l}_{u_i}$ defined as follows:

$$\mathbf{l}_{u_i} = \mathbf{p} - \mathbf{a}_i - \mathbf{c}_i - \mathbf{R}_{\mathbf{z}_b}(\alpha_i)\mathbf{R}_{\mathbf{y}_{pul_i}}(\beta_i)(\mathbf{h}_i + \mathbf{R}_{\mathbf{y}_{pul_i}}(\theta_i)\mathbf{d}_i) \quad \text{for } i = 1, \dots, m \tag{12}$$

Where $\mathbf{R}_{\mathbf{z}_b}(\alpha_i)$ is the rotation matrix about the $\mathbf{z}_b$ axis of magnitude α_i, $\mathbf{R}_{\mathbf{y}_{pul_i}}(\beta_i)$ and $\mathbf{R}_{\mathbf{y}_{pul_i}}(\theta_i)$ are the rotation matrices about the $\mathbf{y}_{pul_i}$ axis of magnitude β_i and θ_i, respectively. l_{d_i} is 2-norm of vector $\mathbf{l}_{d_i}$ defined as follows:

$$\mathbf{l}_{d_i} = \mathbf{a}_i + \mathbf{R}_{\mathbf{z}_b}(\alpha_i)\mathbf{R}_{\mathbf{y}_{pul_i}}(\beta_i)(\mathbf{h}_i + \mathbf{R}_{\mathbf{y}_{pul_i}}(\gamma_i)\mathbf{k}_i) \quad \text{for } i = 1, \dots, m \tag{13}$$

Where $\mathbf{R}_{\mathbf{y}_{pul_i}}(\gamma_i)$ is the rotation matrix about the $\mathbf{y}_{pul_i}$ axis of magnitude γ_i. The total cable's lengths L_{T_i} determined with the inverse geometric model is used in the direct geometrico-catenary model which takes into account the mechanical behaviour of the cables.

2.2 Direct geometrico-catenary model with uncertainties on the Young's modulus

For large-scale application the elasticity and sagging of the cables cannot be neglected. For smaller applications the direct geometric model is simplified. Theses simplifications make it easier to solve the direct geometric model which is used to control of the MP position in workspace [31]. For larger CDPRs, it is therefore necessary to quantify the MP's maximum position error when cable deformation is neglected. In addition, the uncertainties about the elastic behaviour of the cables require that the Young's modulus is considered to be non-constant and different from one cable to another.

2.2.1 Irvine's model for dead and useful cable length

In this section, Irvine's model [32] is used twice for each cable, on the dead and on the useful cable's length. Figure 3 shows the two parts of the sagging cable.

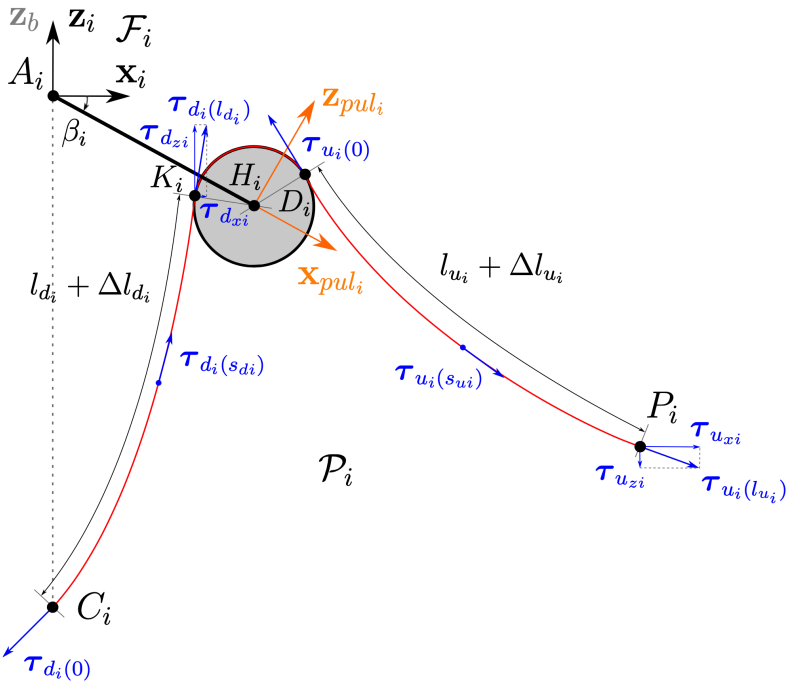

Fig. 3: Deflection of the dead and useful cable length

The i^{th} cable moves in $\mathcal{P}_i$ vertical plane, with $i = 1, \ldots, m$. The cable frame $\mathcal{F}_i$ is attached to this plane. $\mathcal{F}_i$ shares its $\mathbf{z}_i$ axis with the $\mathbf{z}_b$ axis of the base frame $\mathcal{F}_b$. The rotation between $\mathcal{F}_i$ and $\mathcal{F}_b$ is obtained around the axis $\mathbf{z}_i$ and is of magnitude α_i. The dead length's curvilinear abscissa is s_{di} and the useful length's curvilinear abscissa is s_{ui}. The limits of these curvilinear abscissae are given in Eq.(14) for $i = 1, \ldots, m$.

$$\begin{cases} 0 \geq s_{di} \geq l_{d_i} \\ 0 \geq s_{ui} \geq l_{u_i} \end{cases} \tag{14}$$

Moreover, the static equilibrium of the cable is given by Eq.(3) and Eq.(15), for $i = 1, \ldots, m$:

$$\begin{cases} \boldsymbol{\tau}_{d_i(l_{d_i})} = \mu_0 g l_{d_i} \mathbf{z}_b - \boldsymbol{\tau}_{d_i(0)} \\ \boldsymbol{\tau}_{u_i(0)} = \mu_0 g l_{u_i} \mathbf{z}_b - \boldsymbol{\tau}_{u_i(l_{u_i})} \end{cases} \tag{15}$$

Where $\mu_0 g l_{d_i}$ is the dead cable's weight and $\mu_0 g l_{u_i}$ is the useful cable's weight. Indeed, μ_0 is the linear mass of the cable and g is the acceleration due to gravity. On the other hand, $\mathbf{x}_{K_i} = [x_{K_i}, 0, z_{K_i}]^T$ is the position vector of the point K_i in the frame $(C_i, \mathbf{x}_i, \mathbf{z}_i)$. The coordinates x_{K_i} and z_{K_i}, for $i = 1, \ldots, m$, are given by Irvine's model Eq.(16):

$$\begin{cases} x_{K_i} = \dfrac{\tau_{d_{xi}} l_{d_i}}{E_i S_0} + \dfrac{|\tau_{d_{xi}}|}{\mu_0 g}\left[\sinh^{-1}\left(\dfrac{\tau_{d_{zi}}}{\tau_{d_{xi}}}\right) - \sinh^{-1}\left(\dfrac{\tau_{d_{zi}} - \mu_0 g l_{d_i}}{\tau_{d_{xi}}}\right)\right] \\ z_{K_i} = \dfrac{\tau_{d_{zi}} l_{d_i}}{E_i S_0} - \dfrac{{l_{d_i}}^2 \mu_0 g}{2 E_i S_0} + \dfrac{1}{\mu_0 g}\left[\sqrt{{\tau_{d_{xi}}}^2 + {\tau_{d_{zi}}}^2} - \sqrt{{\tau_{d_{xi}}}^2 + (\tau_{d_{zi}} - \mu_0 g l_{d_i})^2}\right] \end{cases} \tag{16}$$

Where $\tau_{d_{xi}}$ is the 2-norm of the vector $\boldsymbol{\tau}_{d_{xi}}$ which is the projection of $\boldsymbol{\tau}_{d_i(l_{d_i})}$ on $\mathbf{x}_i$ axis. $\tau_{d_{zi}}$ is the 2-norm of the vector $\boldsymbol{\tau}_{d_{zi}}$ which is the projection of $\boldsymbol{\tau}_{d_i(l_{d_i})}$ on $\mathbf{z}_i$ axis. S_0 and E_i are the parameters of cable i. S_0 is the section of the cable. E_i is the Young's modulus of the i^{th} cable, it should be noted that E_i is considered as linear in Irvine's model. In addition, the $\mathbf{x}_{P_i} = [x_{P_i}, 0, z_{P_i}]^T$ is the vector position of the point P_i in the frame $(D_i, \mathbf{x}_i, \mathbf{z}_i)$. The coordinates x_{P_i} and z_{P_i}, for $i = 1, \ldots, m$, are given by Irvine's model Eq.(17):

$$\begin{cases} x_{P_i} = \dfrac{\tau_{u_{xi}} l_{u_i}}{E_i S_0} + \dfrac{|\tau_{u_{xi}}|}{\mu_0 g}\left[\sinh^{-1}\left(\dfrac{\tau_{u_{zi}}}{\tau_{u_{xi}}}\right) - \sinh^{-1}\left(\dfrac{\tau_{u_{zi}} - \mu_0 g l_{u_i}}{\tau_{u_{xi}}}\right)\right] \\ z_{P_i} = \dfrac{\tau_{u_{zi}} l_{u_i}}{E_i S_0} - \dfrac{{l_{u_i}}^2 \mu_0 g}{2 E_i S_0} + \dfrac{1}{\mu_0 g}\left[\sqrt{{\tau_{u_{xi}}}^2 + {\tau_{u_{zi}}}^2} - \sqrt{{\tau_{u_{xi}}}^2 + (\tau_{u_{zi}} - \mu_0 g l_{u_i})^2}\right] \end{cases} \tag{17}$$

Where $\tau_{u_{xi}}$ is the 2-norm of the vector $\boldsymbol{\tau}_{u_{xi}}$ which is the projection of $\boldsymbol{\tau}_{u_i(l_{u_i})}$ on $\mathbf{x}_i$ axis. $\tau_{u_{zi}}$ is the 2-norm of the vector $\boldsymbol{\tau}_{u_{zi}}$ which is the projection of $\boldsymbol{\tau}_{u_i(l_{u_i})}$ on $\mathbf{z}_i$ axis. Moreover, the $\mathbf{x}_{K_i}$ and $\mathbf{x}_{P_i}$ vectors, for $i = 1, \ldots, m$, can be expressed as a function of $\mathbf{l}_{d_i}$ Eq.(13) and $\mathbf{l}_{u_i}$ Eq.(12), respectively:

$$\begin{cases} \mathbf{x}_{K_i} = \mathbf{R}_{\mathbf{z}_b}^{-1}(\alpha_i)\mathbf{l}_{d_i} \\ \mathbf{x}_{P_i} = \mathbf{R}_{\mathbf{z}_b}^{-1}(\alpha_i)\mathbf{l}_{u_i} \end{cases} \tag{18}$$

2.2.2 Optimization problem to solve the direct geometrico-catenary model

Solving the direct geometrico-catenary model is similar to solving the inverse geometric model Eq.(10). However, different constraints must me added : the cable's static equilibrium Eq.(15), the cable's deformation Eq.(18) and the L_{T_i} Eq.(11). The total cable's length L_{T_i} is known thanks to the inverse geometric model, but not its different parts, i.e. l_{d_i}, l_{u_i} and $r_{p_i}(\gamma_i - \theta_i)$ the length of the cable wounded on the pulley. It is then possible to determine the MP position with the optimization problem Eq.(10), but with the following additional constraints:

$$\begin{cases} \boldsymbol{\tau}_{d_i(0)} + \boldsymbol{\tau}_{d_i(l_{d_i})} - \mu_0 g l_{d_i} \mathbf{z}_b = \mathbf{0} \\ \boldsymbol{\tau}_{u_i(0)} + \boldsymbol{\tau}_{u_i(l_{u_i})} - \mu_0 g l_{u_i} \mathbf{z}_b = \mathbf{0} \\ \mathbf{x}_{K_i} - \mathbf{R}_{\mathbf{z}_b}^{-1}(\alpha_i)\mathbf{l}_{d_i} = \mathbf{0} \\ \mathbf{x}_{P_i} - \mathbf{R}_{\mathbf{z}_b}^{-1}(\alpha_i)\mathbf{l}_{u_i} = \mathbf{0} \\ l_{u_i} + l_{d_i} + r_{p_i}(\gamma_i - \theta_i) - L_{T_i} = 0 \end{cases} \tag{19}$$

In this case the system unknowns are:

$$[\mathbf{p}, \boldsymbol{\tau}_{u_i(0)}, \boldsymbol{\tau}_{u_i(l_{u_i})}, \boldsymbol{\tau}_{d_i(0)}, \boldsymbol{\tau}_{d_i(l_{d_i})}, \mathbf{f}_{c_i}, \mathbf{f}_{p_i}, \mathbf{h}_i, \mathbf{d}_i, \mathbf{k}_i] \quad \text{for } i = 1, \ldots, m \tag{20}$$

Where $\mathbf{p}$ is now the new MP's position vector in $\mathcal{F}_b$ after resolving the direct geometrico-catenary model. This optimization problem is also solved with the Matlab function "*fmincon*". The initialization of the optimization problem is done with the tensions and geometrical configurations obtained by solving the inverse geometric model Eq.(10).

2.2.3 Variations in Young's modulus of cables

In CDPRs the cables are repeatedly loading and unloading. Due to the inter-wire sliding friction constituting the cables, the elastic behaviour of the cables is non-linear. The cables elasticity is subject to a hysteresis loop [33,34]. In addition, the trajectory history of the MP has an influence on the loading or unloading status of the cables. It is therefore very difficult to know whether the cables have been stretched or relaxed longitudinally. In order to consider the uncertainty on the cable elasticity in Irvine's model, Young's modulus E is considered to be non-constant and different between cables. E_i, for $i = 1, \ldots, m$, is bounded between a minimum and maximum value Eq.(21).

$$E_{min} \geq E_i \geq E_{max} \tag{21}$$

According to ISO 12076, a cable must work between 10% and 30% of its breaking load τ_{lim}. However, a cable installed on a CDPR does not necessarily work in this interval. In addition, the European ISO 4309: 2010 specifies that for a standardised cable the elastic limit is higher than 60% of τ_{lim}. In this paper, it is considered that the cables work between 5% and 50% of τ_{lim}. Considering the experimental results presented in [26] and by extrapolating the values between 5% and 50% of τ_{lim}, an uncertainty of $\pm 30\%$ of nominal Young's modulus is determined. For a steel wire cable this uncertainty allows to cover the whole range of variation of the elasticity. The nominal Young's modulus E_{nom} is defined by Eq.(22).

$$E_{nom} = l_{init} \frac{0.5\tau_{lim} - 0.05\tau_{lim}}{S_0 \Delta l} \tag{22}$$

Where Δl is the cable elongation between a loading of 5% and one of 50% of τ_{lim}. l_{init} is the initial cable length at 5% of τ_{lim}. E_{min} and E_{max} are defined as follows:

$$\begin{cases} E_{min} = 0.7 E_{nom} \\ E_{max} = 1.3 E_{nom} \end{cases} \tag{23}$$

2.3 Strategy to determine the MP'smaximum position error

The aim is twofold, firstly to quantify the MP's position error when the cable deformation is neglected. Secondly to quantify the MP's position uncertainty when the Young's modulus is non-constant. Finally to check whether these errors are acceptable for large-scale AM applications or not. The MP's position error Δp is defined by the 2-norm of the vector $\Delta \mathbf{p}$. Figure 4 shows $\Delta \mathbf{p}$ which is the difference between the desired theoretical position $\mathbf{p}_{ini}$ and the true position $\mathbf{p}$ of the MP.

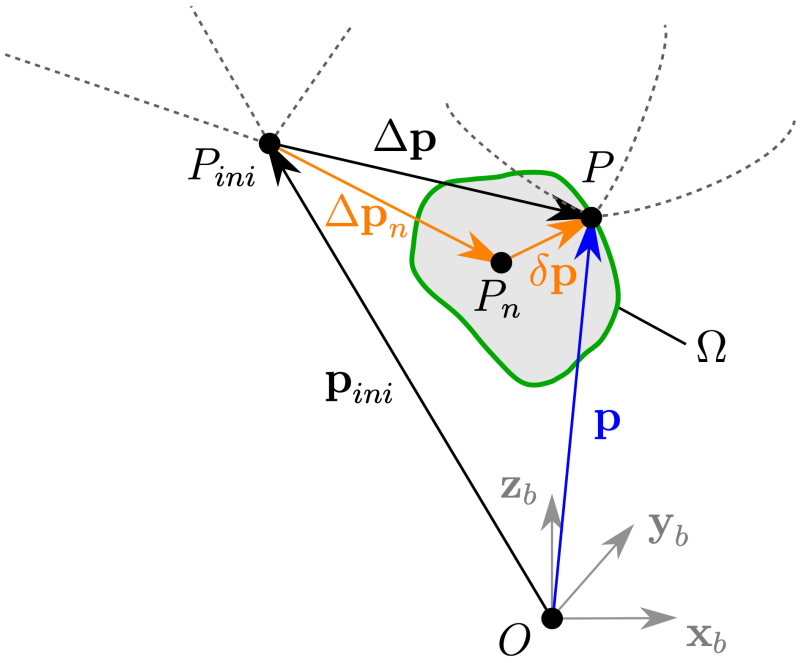

Fig. 4: MP position error $\Delta \mathbf{p}$

The $\Delta \mathbf{p}_n$ vector represents the MP's position variation when the cable's deformation is neglected in the inverse geometric model and the Young's modulus is equal to E_{nom} in the direct geometrico-catenary model. Moreover, the

variation of Young's moduli E_i, for $i = 1, \ldots, m$, creates an uncertainty area around the point P_n which is named Ω. $\delta\mathbf{p}$ vector represents the MP's position uncertainty when the E_i varies independently between E_{min} and E_{max}. $\Delta\mathbf{p}$ can be formulated as follows:

$$\Delta\mathbf{p} = \mathbf{p} - \mathbf{p}_{ini} = \Delta\mathbf{p}_n + \delta\mathbf{p} \tag{24}$$

In addition to solving the direct geometrico-catenary model (cf. Eq.(10) and Eq.(19)), the maximum position error Δp_{max} can be determined by solving the following optimization problem:

$$\begin{cases} \Delta p_{max} = \min(-\Delta p) \\ constraints: \\ E_i \geq E_{min} \\ E_i \leq E_{max} \end{cases} \tag{25}$$

3 CDPR architecture studied

In this part, the mechanical design of the universal joint pulley is detailed with Computer Aided Design (CAD) modelling. Then, the dimensions of the geometrical parameters are determined in order to use the suspended CDPR in large-scale AM applications. In addition, a stress analysis validates the statement [21] that the universal joint pulley reduces the baseplate's and lever arm's mechanical stress.

3.1 Mechanical design

3.1.1 CAD modelling of universal joint pulley

Universal joints are available in a wide variety of shapes, sizes and configurations to accommodate to many mechanical applications. The difficulty to use an universal joint for a CDPR pulley is the large magnitude of the two angles α_i and β_i. Figure 5 shows the CAD modelling of the universal joint pulley designed with CATIA software.

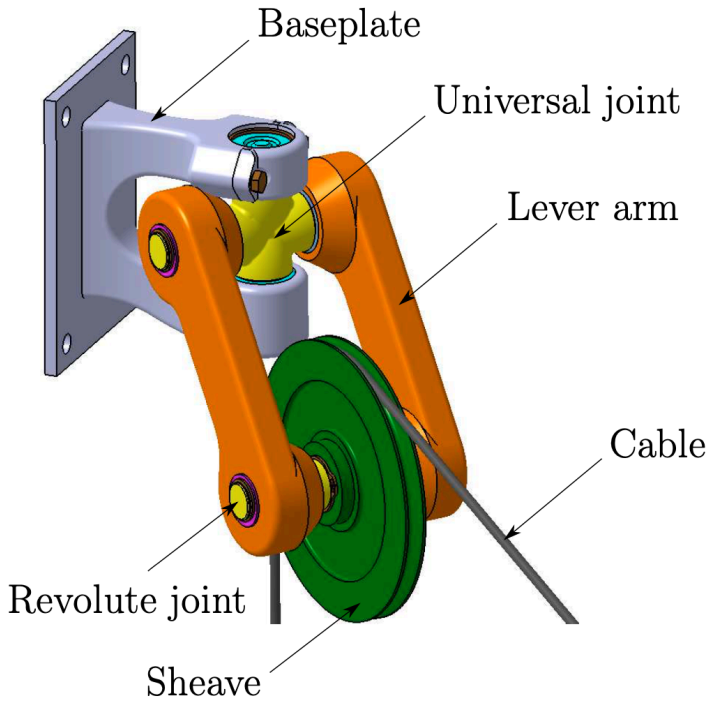

Fig. 5: CAD modelling of the universal joint pulley

The shapes have been designed to avoid part collisions for a 90 degrees magnitude of the angles α_i and β_i. The material used for the different parts (baseplate, lever arm and sheave) is Aluminium alloy 6063. To limit friction, the three revolute joints are made of six needle bearings, four for the universal joint and two between the sheave and the lever arm. A ball thrust bears the vertical load. To dimension the cable, the usual rule is that the ratio between the sheave radius r_p and the cable radius must be higher than 20. On average, a $2mm$ radius steel wire cable can withstand $10kN$. This is more than enough for large-scale AM applications. As a result, the sheave radius r_p is chosen set at $50mm$. In addition, to avoid interference between the sheave and other parts of the pulley, the lever arm must be longer than r_p. In this paper the lever arm length of the pulley is set at $104mm$. The weight of the moving parts, i.e. all parts constituting the assembly of the lever arms with the sheave, is therefore $6.85N$. Finally, in the pulley frame $\mathcal{F}_{pul_i}$, the gravity center G_i is positioned, in mm, at the following coordinates $(-33.4, 0, 0)$.

3.1.2 CDPR architecture for large-scale AM applications

The suspended CDPR architecture can be adapted to AM for construction. Indeed, the main advantages are to have a large regular workspace and to be

easily reconfigurable according to the environment and the shapes that need to be manufactured. The idler pulleys are attached to pillars. A maximum of four pillars is needed in order to limit their number in situ and to have a parallelepipedic regular workspace. Without loss of generality, for this study there is only one cable on each pillar. In this paper, the dimensions of the CDPR are chosen to be 15x15x15m in order to be able to have large-scale AM applications. Figure 6 shows the complete CAD modelling of the CDPR.

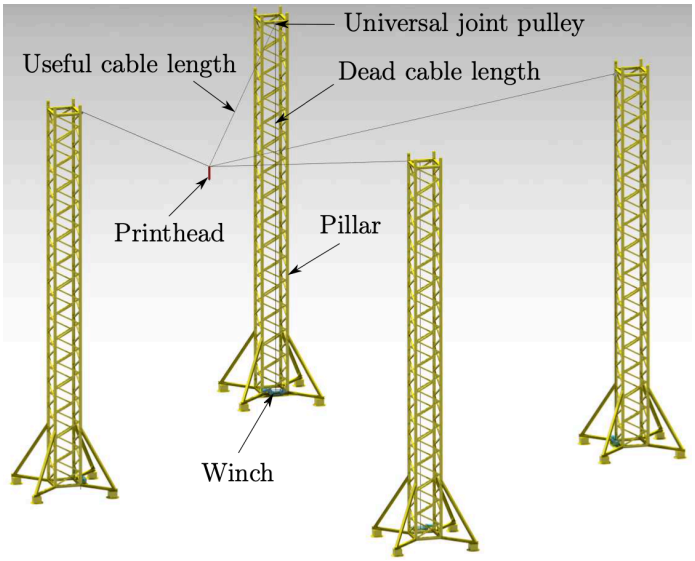

Fig. 6: CAD modelling of the CDPR for large-scale AM applications with $\mathbf{p}_{ini} = [-2.25, -6.75, 13]^T$ in m

Moreover, the pillars are locked to the ground on concrete blocks to prevent them from tipping over. The winches are at ground level for an easy installation. The dead cable lengths are near the pillars for safety. Finally, the pulleys are oriented to have a ± 45 degrees magnitude of the angles α_i.

3.2 Stress analysis on the lever arm of a pulley.

After the CAD modelling of the pulley and CDPR, a stress analysis is performed on the baseplate of the pulley with the ABAQUS software. To perform this stress analysis, the cable tensions applied to the pulley are calculated for the position $\mathbf{p}_{ini} = [-2.25, -6.75, 13]^T$ in m and a mass of 200kg is applied to the MP. Figure 7 shows the iso-chromes of the equivalent von Mises stress for the highest loaded pulley. Parts of the pulley not shown in Figure 7 are considered as rigid bodies. The results shows that the stresses are relatively low in the lever arms compared to the baseplate.

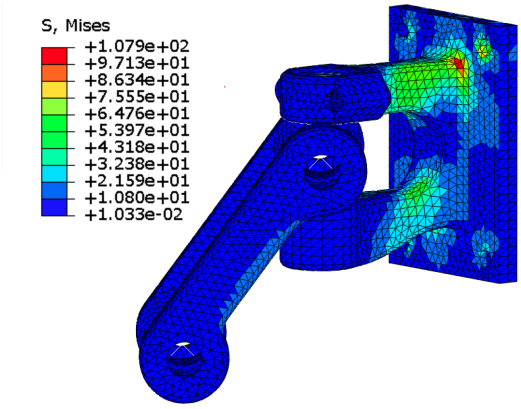

Fig. 7: Iso-chromes of the von Mises equivalent stress for the baseplate of the universal joint pulley

The maximum von Mises stress is in the baseplate and is equal to $107.9MPa$, which is lower than the elastic limit of Aluminium alloy 6063 which is $160MPa$. The results obtained from the stress analysis are compared to those obtained with a conventional pulley. This pulley has only one revolute joint to the baseplate. The lever arm therefore moves in a horizontal plane. In order to maintain similar shapes, the second rotation of the universal joint is blocked with splines. The dimensions of the geometrical parameters are the same as the universal joint pulley, i.e. $r_p = 50mm$ and the lever arm length is equal to $104mm$. Finally, the loading case is determined for the same position $\mathbf{p}_{ini} = [-2.25, -6.75, 13]^T$ in m. Figure 8 shows the CAD modelling of a conventional pulley (a) and the results of the stress analysis (b).

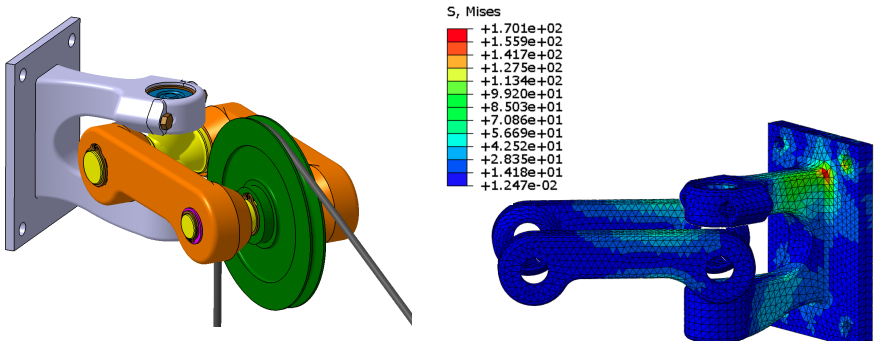

(a) (b)

Fig. 8: (a) CAD modelling of a conventional pulley; (b) Stress analysis on the baseplate of the conventional pulley

The results show that the baseplate of the universal joint pulley is less stressed than the baseplate of the conventional pulley. Indeed, the maximum von Mises stress for the conventional pulley is $170.1MPa$. Note that this is higher than the elastic limit of the 6063 aluminium alloy. In addition, the lever arms of the conventional pulley are more stressed, especially in bending. In conclusion, for the same materials and part geometries, the universal joint pulley will deform less than the conventional pulley. It should be noted that the deformation of the pulleys necessarily causes a variation in the actual position of the MP.

4 Analysis of the MP position errors in static workspace

This part focuses on quantifying the MP position errors using the methodology of section 2 and the CDPR design defined in section 3. First, the accessible static workspace is determined from a geometrical point of view with limits set for the tension in the cables. Then, the largest and the smallest Δp_{max} is determined and located in this accessible static workspace. In addition, the uncertainty area Ω is determined for these two positions. Secondly, the MP position errors are calculated on a helical trajectory and on a horizontal plane. It is then possible to check whether a large-scale AM application is feasible or not.

4.1 Analysis of the largest and smallest Δp_{max}

First, the accessible static workspace is determined by avoiding collisions in the pulleys and by checking that the minimum and maximum cable tensions are not exceeded. The steel wire cables used are Carl Stahl Technocables Ref 1692. The breaking load is $\tau_{lim} = 10.29kN$ and the linear mass is $\mu_0 = 3.10^{-5}kg/mm$. The minimum and maximum cable tensions are therefore equal to $0.51kN$ and $5.15kN$, respectively. Furthermore, it has been shown experimentally in [26] that this cable has an E_{nom} equal to $102.2Gpa$. With Eq. 23, the uncertainty of the Young's moduli is defined by the following bounds: $E_{min} = 71.5GPa$ and $E_{max} = 132.8GPa$. Recall that a mass of $200kg$ is applied to the MP. Figure 9 shows the accessible static workspace for the CDPR studied as well as the initial points P_1 and P_2 which correspond to the smallest and largest Δp_{max}, respectively.

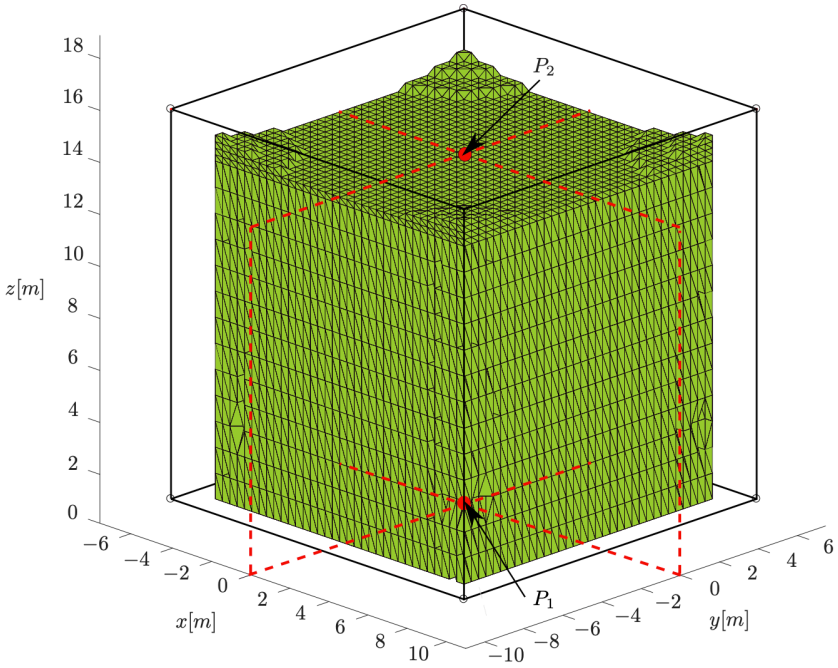

Fig. 9: Accessible static workspace and location of the smallest and largest Δp_{max}

In this workspace the largest maximum MP position error Δp_{max} is equal to $302.6mm$ and is located in the base frame $\mathcal{F}_b$ at coordinates $\mathbf{p}_{ini} = [0, 0, 13.25]^T$ in m, see point P_2 in figure 9. The smallest Δp_{max} is equal to $29.3mm$ and is at ground level at coordinates $\mathbf{p}_{ini} = [0, 0, 0]^T$ in $\mathcal{F}_b$, see point P_1 in figure 9. For these two positions, Table 1 shows the values of Δp_n and δp for the largest and smallest Δp_{max}. Where Δp_n is the 2-norm of $\Delta \mathbf{p}_n$ and represents the error when the cable deformation is neglected in the inverse geometric model. And δp is the 2-norm of $\delta \mathbf{p}$ and represents the uncertainty of the MP position when the Young's modulus is considered as not constant in the direct geometrico-catenary model.

Table 1: Δp_n and δp values for the largest and smallest Δp_{max} in accessible static workspace

MP position in $\mathcal{F}_b$ [m]	Δp_{max} [mm]	Δp_n [mm]	δp [mm]
$P_1 = [0, 0, 0]^T$	29.3	19.5	9.8
$P_2 = [0, 0, 13.25]^T$	302.6	214.6	88.3

According to the results in Table 1, the error Δp_n due to cable sagging and elasticity is much larger than the uncertainty δp due to the variation of Young's moduli of the cables. Furthermore, it is interesting to compare the different uncertainty areas Ω for each initial point P_1 and P_2. Figure 10 shows the uncertainty area Ω for the largest and smallest Δp_{max} in accessible static workspace.

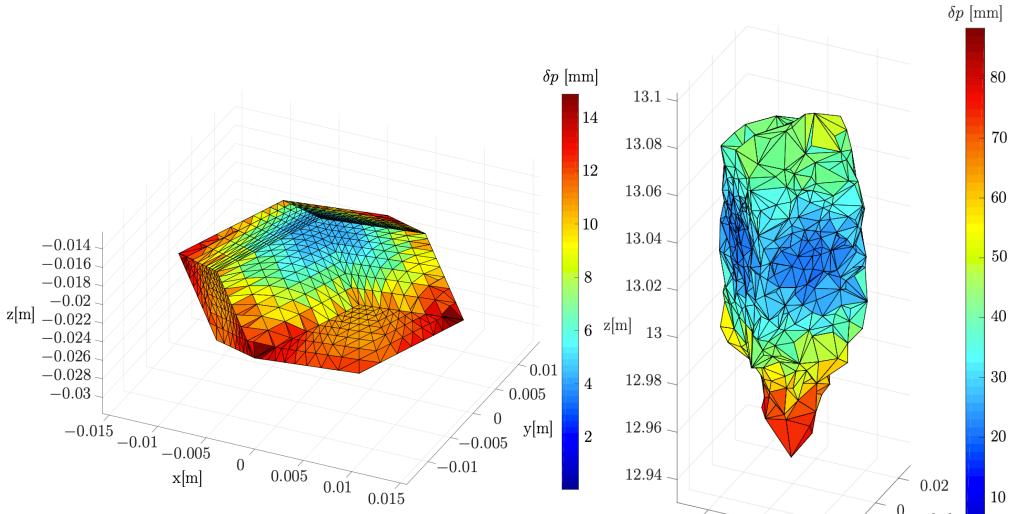

(a) Ω for P_1 the smallest Δp_{max}

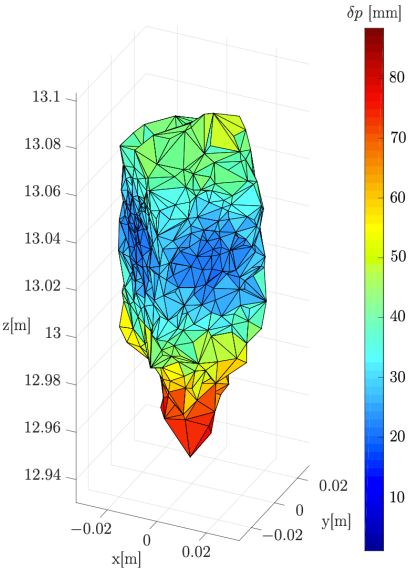

(b) Ω for P_2 the largest Δp_{max}

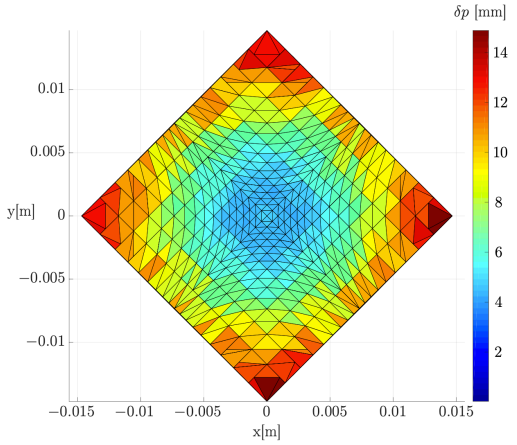

(c) Top view of Ω for P_1 the smallest Δp_{max}

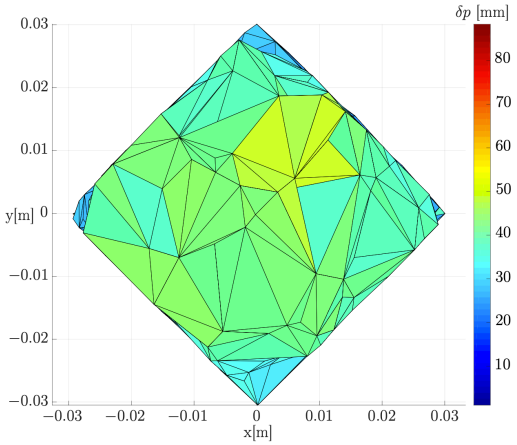

(d) Top view of Ω for P_2 the largest Δp_{max}

Fig. 10: Uncertainty areas Ω for the largest and smallest Δp_{max}

In Figure 10 the colour gradient corresponds to the δp value. Figures 10a and 10b show that the uncertainty area Ω at ground level is much smaller than at the top of the accessible static workspace. Indeed, the volume of Ω for the smallest Δp_{max} is equal to $3.126 \times 10^{-6} m^3$ while the volume of Ω for the largest Δp_{max} is equal to $1.513 \times 10^{-4} m^3$. It can be deduced from this that it is not specifically the length of the cables that increases the uncertainty area Ω, but the large tensions in cables. Indeed, the tensions are more and more important when the MP increases its altitude along the $\mathbf{z}_b$ axis. Finally, despite the different geometrical shapes of the two Ω, Figures 10c and 10d show that the projection of Ω in the $(O, \mathbf{x}_b, \mathbf{y}_b)$ plane is always square.

4.2 MP accuracy on a helical trajectory

In AM, a large error can result in poor part quality, but more importantly, it can damage the printhead. It is therefore important to quantify this error. In this part, the quantification of the MP position error is performed on a helical trajectory as a helical trajectory is representative of a construction by AM. Figure 11 shows the theoretical helical trajectory and the maximum trajectory error represented by Δp_{max}.

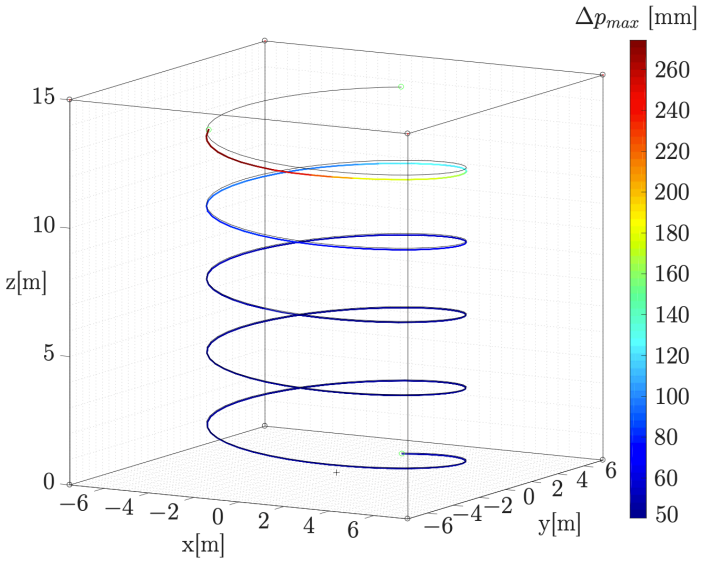

Fig. 11: Δp_{max} on an helical trajectory

Along the trajectory, Δp_{max} ranges from $50mm$ to $270mm$. Δp_{max} is the lowest at the bottom of the static workspace. Figure 12 shows that the variation in Δp_{max} is small in the lower half of the static workspace. This observation is an advantage for the large-scale AM. Furthermore, it is interesting

to analyse the components of the $\Delta\mathbf{p}_{max} = [\Delta p_x, \Delta p_y, \Delta p_z]^T$ vector along the helical trajectory. Figure 12 shows the evolution of the components of the $\Delta\mathbf{p}_{max}$ vector as a function of height in the static workspace.

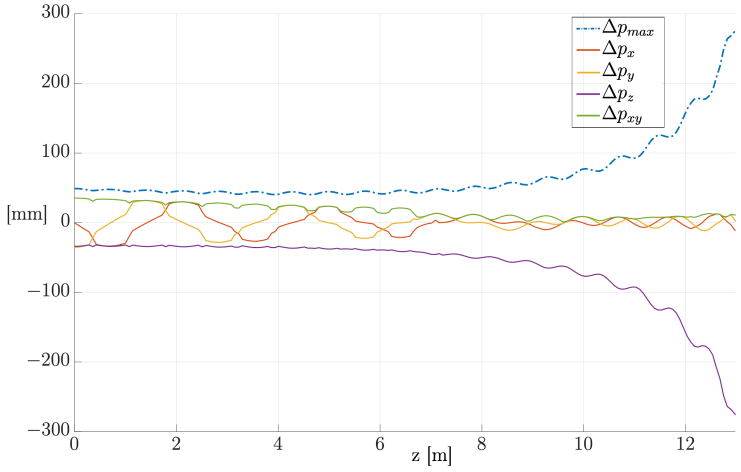

Fig. 12: Evolution on helical trajectory of the components of $\Delta\mathbf{p}_{max}$ and its 2-norm Δp_{max}

In Figure 12, Δp_{xy} is the 2-norm of the Δp_x and Δp_y components which quantifies the MP horizontal positioning error. In Figure 12, at the bottom of the static workspace, the horizontal error Δp_{xy} and the vertical error Δp_z are of the same order of magnitude. The higher the MP goes in the static workspace, the smaller Δp_{xy} becomes. Conversely, Δp_z increases, especially above $7.5m$ in height. The results in Figure 12 confirm that the Δp_{max} error is close to a constant on the lower half of the static workspace. As a result, for a $15m$ high CDPR, it is better to avoid the AM construction being higher than $7.5m$.

4.3 MP accuracy on a horizontal plane

In this part, the quantification of the MP position error is performed on horizontal planes. These planes are chosen at the ends of the lower half of the CDPR, i.e. at $0m$ and $7.5m$. The aim is to determine the error on the vertical axis $\mathbf{z}_b$. To do this, the minimum and maximum vertical error of $\Delta\mathbf{p}$, i.e. $\Delta p_{z\,min}$ and $\Delta p_{z\,max}$, must be found for each point of the plane studied. It is then possible to draw two error surfaces, one for $\Delta p_{z\,min}$ and one for $\Delta p_{z\,max}$. The area between these surfaces represents the uncertainty area of the MP position. Figures 13a and 13b show the vertical error surfaces for theoretical

MP positions belonging to the horizontal plane at ground level and at $7.5m$, respectively.

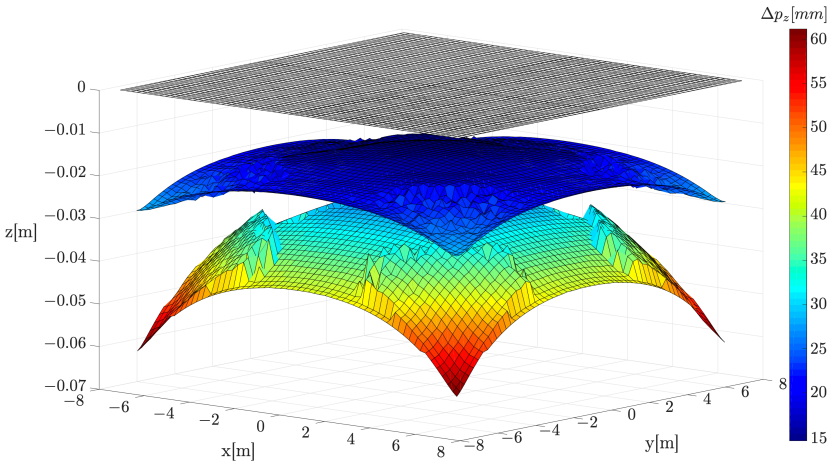

(a) Δp_z at $0m$

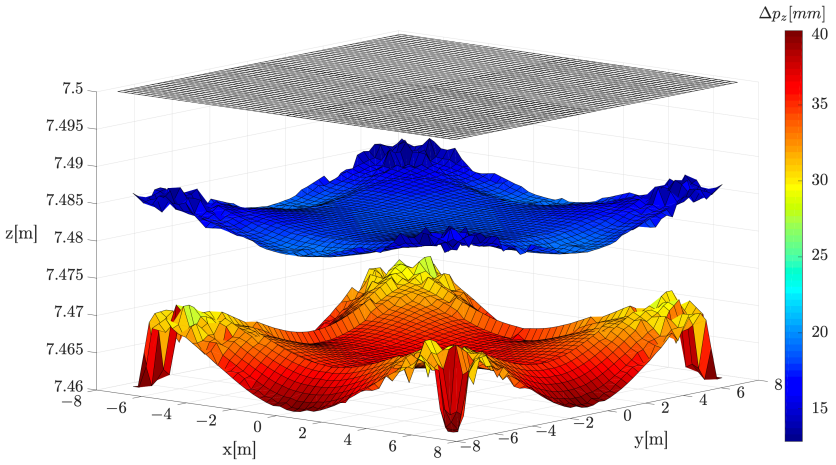

(b) Δp_z at $7.5m$

Fig. 13: Vertical error surfaces $\Delta p_{z_{min}}$ and $\Delta p_{z_{max}}$ for theoretical MP positions belonging to the horizontal plane at ground level (a) and at $7.5m$ (b)

Figure 13 shows that on the studied planes, the maximum vertical positioning error $\Delta p_{z_{max}}$ is equal to $61mm$ at $0m$ hight and equal to $40mm$ at $7.5m$ hight. These errors, which are only the vertical component, can be problematic for large-scale construction in AM. Nevertheless, these errors can be reduced by taking into account the deformation of the cables (sagging and elasticity) with the E_{nom} (cf. Eq. 22) in the CDPR model. However, as the true Young's moduli values of the cables are very difficult to quantify in real time, there will always be an uncertainty δp (see Fig. 4). The maximum value of δp is calculated numerically in the lower half of the CDPR and is equal to $28mm$. This maximum uncertainty δp on the repeatability of printhead positioning is relatively acceptable for large-scale AM construction with a CDPR of $15 \times 15 \times 15m$.

5 Conclusion

This paper deals with the accuracy of Cable-Driven Parallel Robots (CDPRs) equipped with an universal joint pulley for large-scale Additive Manufacturing (AM) applications. Geometrico-catenary models with uncertainty in the Young's moduli of the cables are compared with conventional geometric models. Based on these models, a method for analyzing the positioning error Δp of the Mobile Platform (MP) is detailed. Next, the detailed mechanical design of the universal joint pulley is presented as well as the overall $15 \times 15 \times 15m$ structure of the CDPR. The universal joint pulley is compared to a conventional pulley using a stress analysis. The results show that the universal joint pulley used for large-scale applications minimizes the mechanical stresses. Finally, the accuracy of the MP is investigated in the accessible static workspace. For this purpose, the positions where the positioning error Δp_{max} is minimum and maximum are identified. On these positions, the uncertainty area Ω due to the variation of the Young's moduli of the cables is determined. The results show that the volume of Ω increases at the top of the accessible static workspace where the cable tensions are the highest. Then, the positioning error Δp_{max} of the MP is analyzed on a helical trajectory representative of an AM application. It is found that Δp_{max} is lowest and close to a constant on the lower half of the CDPR. It should be noted that the higher the MP altitude is, the vertical error Δp_z increases, but conversely the horizontal error Δp_{xy} decreases. Finally, on two horizontal theoretical planes, the minimum vertical error $\Delta p_{z_{min}}$ and maximum vertical error $\Delta p_{z_{max}}$ are quantified. All the results in section 4 show that, for the studied CDPR, if the deformation of the cables is not taken into account then the positioning error is too large for a large-scale AM application. However, if the geometrico-catenary model developed in section 2 is used to determine the length of the cables, then the positioning error of the printhead is greatly reduced. Only the δp uncertainty remains due to the variation of the Young's moduli. Finally, the δp uncertainty in the lower half of the accessible static workspace is determined to be less than $28mm$. This printhead positioning error is relatively acceptable for large-scale AM applications for construction.

References

1. K. V. Wong, A. Hernandez, A Review of Additive Manufacturing, ISRN Mechanical Engineering, (2012)
2. A. Diourté, F. Bugarin, C. Bordreuil, S. Segonds, Continuous three-dimensional path planning (CTPP) for complex thin parts with wire arc additive manufacturing , Additive Manufacturing, pp.101622, (2020)
3. N.D. Watson, N.A. Meisel, S.G. Bilén, J. Duarte, S. Nazarian, Large-scale additive manufacturing of concrete using a 6-axis robotic arm for autonomous habitat construction, An Additive Manufacturing Conference, (2019)
4. K. Subrin, T. Bressac, S. Garnier, A. Ambiehl, E. Paquet, B. Furet, Improvement of the mobile robot location dedicated for habitable house construction by 3D printing, International Federation of Automatic Control, (2018)
5. N. Binaud, S. Caro, P. Wenger, Comparison of 3-RPR planar parallel manipulators with regard to their kinetostatic performance and sensitivity to geometric uncertainties, Meccanica, vol.46, (2011)
6. B. Duan, A new design project of the line feed structure for large spherical radio telescope and its nonlinear dynamic analysis, Mechatronics, vol.9(1), pp.53–64, (1999)
7.] L. Gagliardini, S. Caro, M. Gouttefarde, A. Girin, Discrete reconfiguration planning for cable-driven parallel robots, Mechanism and Machine Theory, vol.100, pp. 313–337, (2016)
8. S. Qian, K. Bao, B. Zi, N. Wang, Kinematic Calibration of a Cable-Driven Parallel Robot for 3D Printing, Sensors, vol.18, (2018)
9. B. Zi, N. Wang, S. Qian, K. Bao, Design, stiffness analysis and experimental study of a cable-driven parallel 3D printer, Mechanism and Machine Theory, vol.132, pp.207-222, (2019)
10. E. Barnett, C. Gosselin, Large-Scale 3D Printing With A Cable-Suspended Robot, Additive Manufacturing, vol.7, (2015)
11. J.-B. Izard, A. Dubor, P.-E. Herve, E. Cabay, D. Culla, M. Rodriguez, M. Barrado, Large-scale 3D printing with cable-driven parallel robots, Construction Robotics, vol.1, pp.69-76, (2017)
12. P.T. Tuong, T.T. Nguyen, Using a Cable-Driven Parallel Robot with Applications in 3D Concrete Printing, Applied Sciences, vol.11(2), pp.563, (2021)
13. N. Zhang, W. Shang, Dynamic trajectory planning of a 3-dof under-constrained cable-driven parallel robot, Mechanism and Machine Theory, vol.98, pp.21-35, (2016)
14. N. Riehl, M. Gouttefarde, S. Krut, C. Baradat, F. Pierrot, Effects of non-negligible cable mass on the static behavior of large workspace cable-driven parallel mechanisms, IEEE International Conference on Robotics and Automation, pp. 2193–2198, (2009)
15. G. Abbasnejad, M. Carricato, Real solutions of the direct geometrico-static problem of under-constrained cable-driven parallel robots with 3 cables: a numerical investigation, Meccanica, vol.47, pp.1761–1773, (2012)
16. B. Ouyang, W.-W. Shang, A new computation method for the force-closure workspace of cable-driven parallel manipulators, Robotica, vol. 33(3), pp.537–547, (2015)
17. J. Seon, S. Park, S. Ko, J. Park, Cable configuration analysis to increase the rotational range of suspended 6-DOF cable driven parallel robots, 16th International Conference on Control, Automation and Systems, (2016)
18. H. Yuan, E. Courteille, D. Deblaise, Static and dynamistic stiffness analyses of cable-driven parallel robots with non-negligible cable mass and elasticity, Mechanism and Machine Theory, vol.85, pp.64-81, (2015)
19. D. Nguyen, M. Gouttefarde, O. Company, F. Pierrot, On the simplifications of cable model in static analysis of large-dimension cable-driven parallel robots, International Conference on Intelligent Robots and Systems, (2013)
20. M. Hamann, C. Ament, Calibration procedure for a geometrically reconfigurable 3-DoF cable-driven parallel robot, International Conference Modelling, Simulation and Identification, (2018)
21. T. Paty, N. Binaud, S. Caro, S. Segonds, Cable-Driven Parallel Robot Modelling Considering Pulley Kinematics and Cable Elasticity, Mechanism and Machine Theory, vol.159, (2021)

22. E. Picard, S. Caro, F. Plestan, F. Claveau, Control solution for a cable driven parallel robot with highly variable payload, ASME International Design Engineering Technical Conferences and Computers and Information in Engineering Conference, pp.1429–1436, (2018)
23. E. Picard, S. Caro, F. Claveau, F. Plestan, Pulleys and force sensors influence on payload estimation of cable-driven parallel robots, IEEE/RSJ International Conference on Intelligent Robots and Systems (IROS), pp.1429–1436, (2018)
24. C. Gosselin, M. Grenier, On the determination of the force distribution in over constrained cable-driven parallel mechanisms, Meccanica, vol.46, pp.3–15, (2011)
25. J.-P. Merlet, Some properties of the Irvine cable model and their use for the kinematic analysis of cable-driven parallel robots, Mechanism and Machine Theory, vol.135, pp.271-280, (2019)
26. S. Baklouti, S. Caro, E. Courteille, Sensitivity analysis of the elasto-geometrical model of cable-driven parallel robots, The Third International Conference on Cable-Driven Parallel Robots, (2018)
27. R. Mersi, S. Vali, M. S. haghighi, G. Abbasnejad, M. T. Masouleh, Design and control of a suspended cable-driven parallel robot with four cables, 6th RSI International Conference on Robotics and Mechatronics (IcRoM), pp. 470–475, (2018)
28. M. Gouttefarde, J. Lamaury, C. Reichert, T. Bruckmann, A Versatile Tension Distribution Algorithm for n-DOF Parallel Robots Driven by n + 2 Cables, IEEE Transactions on Robotics, vol.31, pp.1444-1457, (2015)
29. A. F. Cote, P. Cardou, C. Gosselin, A tension distribution algorithm for cable-driven parallel robots operating beyond their wrench-feasible workspace, 16th International Conference on Control, Automation and Systems (ICCAS), pp.68-73, (2016)
30. T. Bruckmann, A. Pott, D. Franitza, M. Hiller, A Modular Controller for Redundantly Actuated Tendon-Based Stewart Platforms, EuCoMes, The First Conference on Mechanism Science, pp.1-12, (2012)
31. A.-B. Alp, S. Agrawal, Cable suspended robots: design, planning and control, Proceedings 2002 IEEE International Conference on Robotics and Automation, vol.4, pp.4275–4280, (2002)
32. H. M. Irvine, Cable Structures, The MIT Press Series in Structural Mechanics, (1981)
33. D. Sauter, P. Hagedorn, On the hysteresis of wire cables in Stockbridge dampers, International Journal of Non-Linear Mechanics, vol.37, pp.1453–1459, (2002)
34. M. Miyasaka, M. Haghighipanah, Y. Li, B. Hannaford, Hysteresis Model of Longitudinally Loaded Cable for Cable Driven Robots and Identification of the Parameters, IEEE International Conference on Robotics and Automation (ICRA), pp. 4051–4057, (2016)